Published in : J Mater Sci (2018), vol. 53, pp. 6135-6146
DOI: 10.1007/s10853-017-1974-9
Status : Postprint (Author's version)

CONTINUOUS-POROUS N-DOPED CARBON NETWORK AS HIGHPERFORMANCE ELECTRODE FOR LITHIUM-ION BATTERIES

Walid Alkarmo[1], Farid Ouhib[1], Abdelhafid Aqil[1], Jean-Michel Thomassin[1], Bénédicte Vertruyen[2], Marie-Laure Piedboeuf[3], Nathalie Job[3], Christophe Detrembleur[1,*], and Christine Jérôme[1,*]

[1] Centre for Education and Research on Macromolecules (CERM), CESAM-RU, University of Liège, Sart-Tilman B6a, 4000 Liège, Belgium
[2] GREENMAT-LCIS, CESAM-RU, Chemistry Department, University of Liège, Sart-Tilman B6b, 4000 Liège, Belgium
[3] Department of Chemical Engineering – Nanomaterials, Catalysis, Electrochemistry, University of Liège, Sart-Tilman B6a,
4000 Liège, Belgium
**Address correspondence to E-mail: christophe.detrembleur@uliege.be; c.jerome@uliege.be*

ABSTRACT

Hierarchical porous N-doped carbon (NPC) is prepared by pyrolysis of poly(methyl methacrylate) (PMMA) particles decorated by graphene oxide (GO) and polypyrrole (PPy) as precursors and used as anode for lithium-ion batteries. The composite precursors with different diameter and composition (PMMA/GO/ PPy-A and B) were conveniently prepared by dispersion polymerization of methyl methacrylate in the presence of graphene oxide as stabilizer in aqueous medium, followed by addition of pyrrole and its oxidative polymerization. After pyrolysis, the resulting NPC composites with hierarchically structured macroand mesopores exhibit high surface area (289–398 m^2/g) and different N-doping levels (7.46 and 4.22 wt% of nitrogen content). The NPC with the highest N-doping level (7.46 wt%) shows high reversible capacities of 831 mAh/g at 74.4 mA/g (C/5) after 50 cycles and excellent rate performances.

Introduction

Lithium-ion batteries (LIBs), among the most wide spread power batteries, have gained increasing attention owing to their potential applications in energy storage devices for portable electronics and smart grids [1]–[3]. Due to their high energy density, high voltage and high cycling stability, the interest in LIBs rapidly expands so as their potential application to electric and hybrid electric vehicles [4]–[6]. At present, the commercial anode materials for LIBs are based on graphitic carbon that presents several advantages including low cost, natural abundance, low lithium-ion (Li^+) potential intercalation and no problem of Li dendrites formation [7]. However, some disadvantages such as low theoretical capacity of graphite (372 mAh/g) and limited rate capability cannot satisfy the increasing need for high-power energy conversion. One of the most important challenges in this technology is to develop new anode materials with higher Li^+ ions storage capacity and high charge/discharge rate capability.

Published in : J Mater Sci (2018), vol. 53, pp. 6135-6146
DOI: 10.1007/s10853-017-1974-9
Status : Postprint (Author's version)

In this context, different candidates based on porous carbons with various microstructure have been investigated as anode in LIBs, such as carbon nanofibers [8], [9], carbon nanotubes (CNT) [10], hollow nanospheres [11], graphene nanosheets [12], [13] and three-dimensional (3D) porous carbons [14]. Among these interesting carbon materials, 3D porous carbons with abundant hierarchical meso/macroporosity are considered as promising materials for energy storage. The 3D porous structure with high surface area can provide multidimensional electron transport pathway, increase the electrode/electrolyte contact, shorten the Li^+ ion transport length and increase their flexibility to better accommodate the strain during the charge/discharge cycles [15], [16].

Another approach to improve the Li^+ storage capacity of carbon-based anodes is via heteroatoms doping (N, S, B, etc.) [17]. Particularly, the incorporation of N atoms in the graphene material has attracted much attention, because of the stronger electronegativity of N atoms than carbon, and the hybridization between the nitrogen lone pair electrons and the graphene π system [18]–[20]. Furthermore, the presence of N atoms increases the carbon intersheets distance and creates a large number of defects which offer more active sites for Li^+ ions insertion [4], [21]. Recently, Liu et al. reported a 2D sandwich architecture of N-doped carbon/reduced graphene oxide (rGO) derived from simple pyrolysis of a polypyrrole associated with GO nanosheets precursor. The obtained porous carbon with high N-doping content exhibits interesting electrochemical lithium storage performances with stable reversible capacity of 669 mAh/g up to 200 cycles at a current density of 100 mA/g [22]. However, despite the beneficial effect of association of N-doped carbon with rGO, it is still challenging to develop novel and scalable approaches for the preparation of continuous-porous N-doped carbon materials, which associate hierarchical meso/macroporous structure with adapted morphology and appropriate N-doping levels for efficient anode material.

In this paper, we report on the easy fabrication of hierarchical meso and macroporous N-doped carbon materials (NPCs) containing graphene. The followed strategy relies on the pyrolysis of poly(methyl methacrylate) nanoparticles stabilized by GO (PMMA/GO) and decorated with polypyrrole as N-doped carbon matrix source (Scheme 1). The synthesis of PMMA/GO particles (step 1 of scheme 1) has already been reported [23] and presents the advantage to avoid the use of additional surfactant, the PMMA particles being stabilized during their formation by the GO sheets. These PMMA particles serve as porous template by thermal degradation. Thanks to the PPy layer, pyrolysis allows to produce porous N-doped carbon materials. This process produces hierarchical meso- and macroporosity as demonstrated by scanning electron microscopy (SEM), developing large surface area as quantified by nitrogen adsorption studies. Finally, the electrochemical performances of these porous carbons were investigated in a half-cell configuration with a lithium disk as counter-electrode and demonstrated strong promise for anode in lithium batteries.

Published in : J Mater Sci (2018), vol. 53, pp. 6135-6146
DOI: 10.1007/s10853-017-1974-9
Status : Postprint (Author's version)

Experimental section

MATERIALS

Methyl methacrylate (MMA; > 99%, Aldrich), α,α´ azoisobutyronitrile (AIBN) (Fluka), Pyrrole (Py, 98%, Aldrich), Iron(III) chloride hexahydrate (≥ 99%, Aldrich) and methanol (99.8%, Aldrich) were used as received. Graphene oxide suspension (GO; N002-PS: 0.5 wt% in water, thickness 1.0–1.2 nm, *x* –*y* dimension ~ 100 nm) was purchased from Angstron Materials.

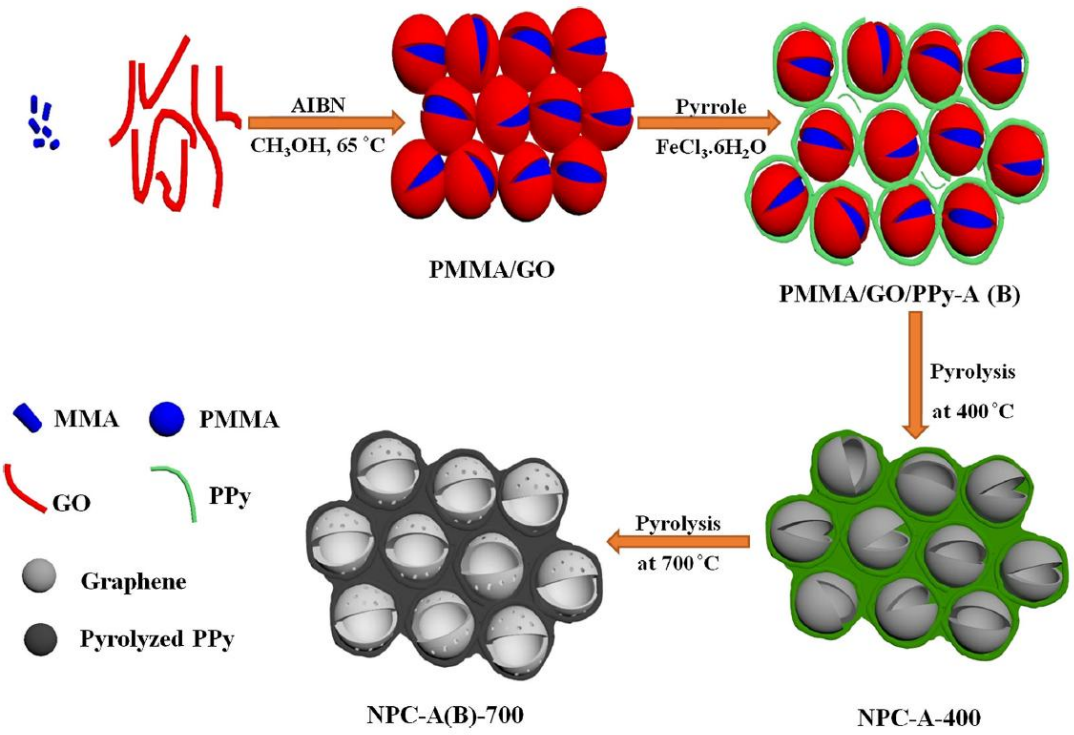

Scheme 1 Strategy of NPCs preparation

SYNTHESIS OF NPCS

SYNTHESIS OF PMMA/GO TEMPLATE

The synthesis of PMMA/GO templates with three different contents of GO, i.e., 1.5, 3 and 6 wt% as compared to PMMA was performed as follows. For the synthesis of PMMA/3 wt% GO, MMA (1 mL, 9.388 mmol) and AIBN (30 mg, 0.182 mmol) were added in a flask containing a mixture of 10 mL of methanol and 6 mL of an aqueous suspension of GO (0.5 wt%). The mixture was degassed with flowing N_2 for 2 min and then stirred at 60 C for 1 h at 1000 rpm. After 30 min, the coloration turned from black to brown with the appearance of PMMA/GO particles. PMMA/3 wt% GO particles are then used as a sacrificial template for preparing the nitrogendoped porous carbon materials. The same

Published in : J Mater Sci (2018), vol. 53, pp. 6135-6146
DOI: 10.1007/s10853-017-1974-9
Status : Postprint (Author's version)

procedure was applied for the synthesis of the PMMA/1.5 wt% GO and PMMA/6 wt% GO, by adding, respectively, 3 or 12 mL of the GO suspension, in place of the 6 mL mentioned above.

SYNTHESIS OF PMMA/GO/PPY-A PRECURSORS

The suspension of PMMA/GO (with 3 wt% of GO) was sonicated by an ultrasonic device for 15 min. Then, pyrrole (60 mg, 0.89 mmol), dissolved in methanol (1 mL), was added to the PMMA/GO suspension under strong stirring (1000 rpm) and the reaction medium was cooled down in an ice bath. $FeCl_3 6H_2O$ (241.7 mg, 0.89 mmol) was then added to the reaction medium. The polymerization of pyrrole was carried out for 12 h at 0 °C. The PMMA/GO/PPy particles were separated from the dispersion by centrifugation (10000 rpm for 10 min) and washed with deionized water. After three successive cycles of dispersion, centrifugation and washing with acidified water, the PMMA/GO/PPy-A particles were then dried at 80 °C for 12 h under vacuum to obtain a black powder.

PMMA/GO/PPy-B precursor was prepared by same procedure by using 120 mg of pyrrole and 442 mg of $FeCl_3 6H_2O$.

PYROLYSIS OF PMMA/GO/PPY PRECURSORS IN NPCS

The final NPC was obtained by pyrolysis of corresponding PMMA/GO/PPy precursors by first heating (5 °C/min) under nitrogen to 400 °C and keeping at this temperature for 60 min. Then, the temperature was increased to 700 C with a heating rate of 5 °C/min under nitrogen and held for 1 h. The obtained NPC is then left to cool down to room temperature under a nitrogen atmosphere.

CHARACTERIZATION

The morphology of the NPC was examined by scanning electron microscopy (SEM; JEOL JSM 840-A) after metallization with Pt (30 nm). The structure was characterized by X-ray diffraction (XRD, Bruker D8 Advance), Raman spectroscopy (LabRAM Aramis) and Fourier transform infrared spectroscopy (FTIR, Perkin Elmer Spectrum BX FTIR instrument). The compression-molded samples were characterized with a transmission electron microscope (TEM; PHILIPS M100) at an accelerating voltage of 100 kV. Thermogravimetric analysis (TGA) was performed on a Q500 machine from TA instruments under a N_2 atmosphere at a heating rate of 5 °C/min. Nitrogen adsorption–desorption measurements were performed to determine the pore texture of the materials [Micromeritics analyzer ASAP 2420 (USA)]. The samples were degassed overnight at 270 °C under high vacuum (133 Pa) prior to measurements. The specific surface area, S_{BET}, was calculated using the Brunauer–Emmett– Teller (BET) equation, with the adsorption data taken in the relative pressure range 0.01–0.10. The micropore volume (V_{DUB}, volume of pores of width lower than 2 nm) was determined by the Dubinin–Radushkevich method.

ELECTROCHEMICAL MEASUREMENTS

Electrochemical characterization of the composites as anode materials in rechargeable lithium-ion batteries was performed at room temperature in a half-cell (CR2032) by galvanostatic charge–

Published in : J Mater Sci (2018), vol. 53, pp. 6135-6146
DOI: 10.1007/s10853-017-1974-9
Status : Postprint (Author's version)

discharge curves at C/5. The working electrodes were prepared by slurry casting on a Cu foil. This electrode consisted of 80 wt% of the active material, 10 wt% of carbon black (Super-P Li from TIMCAL) to enhance the electronic conductivity, 10 wt% of polymer binder (PVDF, polyvinylidene fluoride, Aldrich) and NMP (Nmethyl-2-pyrrolidone) as solvent. Finally, the working electrode was vacuum dried at 80 °C for 12 h. In most of the experiments, the typical mass loading of active electrode material was 0.5 mg/cm^2 and the voltage range was 0.005–1.5 V. However, in many works found in the literature, negative electrode materials are characterized between 0.005 V and 3 V and with higher active material loadings. Therefore, for the material presenting the best performances in the first characterization procedure, the mass loading was further increased to 0.9 mg/cm^2 and the battery was tested in the voltage range of 0.005–3 V. Coin cells were assembled using Li-metal foils as counter and reference electrodes and a microporous polypropylene separator. The cell was soaked by 90 µL of LP71 (1 M $LiPF_6$ in EC:DEC:DMC 1:1:1, Merck). The cell assembly was performed in an Arfilled glove-box. Galvanostatic charge–discharge cycling was performed using a Biologic VMP3 multichannel potentiostat.

Results and discussion

NPCs were synthesized using the polymer templateassisted method, as shown in Scheme 1. First, poly(methyl methacrylate) (PMMA) particles decorated by GO nanosheets (PMMA/GO) are synthesized by free radical polymerization of methyl methacrylate in the presence of dispersed GO as stabilizer in a water/ methanol mixture according to our previous work [23]. In the present work, three different amounts of GO, i.e., 1.5, 3 and 6 wt% compared to PMMA have been used for the synthesis of PMMA particles with the goal to decrease the PMMA particle size and keep them uniform. As previously demonstrated, the GO sheets act as stabilizer and are selectively localized at the surface of the polymer particles. As evidenced by SEM, increasing the GO content from PMMA/ 1.5 wt% GO to PMMA/3 wt% GO decreases the average diameter of the PMMA particles from 600–650 nm to 200–250 nm (Fig. 1a, b). These particles are interconnected probably as a result of aggregation during the drying steps prior to the SEM observations. However, when the GO content is increased further, i.e., to 6 wt% *vs* PMMA, the spherical morphology is completely lost as evidenced by SEM (Fig. 1c). In addition, in order to confirm the localization of the GO at the surface of the PMMA particles, the PMMA/3 wt% GO sample was meltcompressed at 210 °C for 30 s into disks and cut in a thin slice for TEM observation. Figure S1 shows that the GO sheets are dispersed in a regular pattern within the compressed polymer matrix. The average size of the polymer regions surrounded by the GO sheets closely matches the diameter of the particles observed by SEM, which reflects the localization of the GO sheets at the PMMA particles surface prior to compression in accordance with previously reported results [23]. Therefore, the PMMA/GO particles prepared with 3 wt% GO was selected as sacrificial template material for the preparation of porous nitrogen-doped carbon.

Published in : J Mater Sci (2018), vol. 53, pp. 6135-6146
DOI: 10.1007/s10853-017-1974-9
Status : Postprint (Author's version)

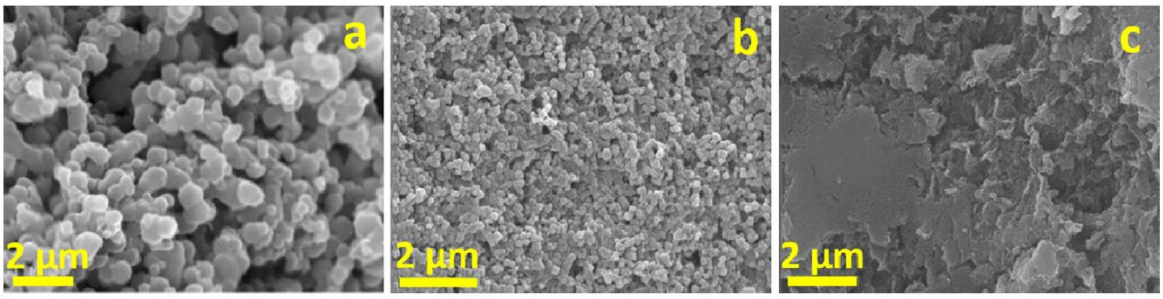

Figure 1 SEM micrograph of PMMA/GO particles obtained with a 1.5, b 3 and c 6 wt% GO (vs. MMA).

In the second step (Scheme 1), pyrrole is added to the suspension of the PMMA/GO particles and polymerized by adding $FeCl_3 6H_2O$ as oxidizing agent without prior drying of the PMMA/GO suspension to avoid particles coagulation. Polypyrrole (PPy) precipitates upon polymerization in the water/ methanol mixture, covering progressively the surface of the PMMA/GO particles, which precipitates in turn because of the formation of the water-insoluble PPy thin coating. Two PMMA/GO/PPy N-doped carbon precursors, PMMA/GO/PPy-A and PMMA/ GO/PPy-B, have been prepared, by adding two times or four times more pyrrole than GO (by weight), respectively. For both samples, the residual iron salts were eliminated out by three repeated dispersion/centrifugation steps in acidified water. After drying, TGA analysis conducted under air confirmed that the residual iron content is below 1% (Figure S2).

The morphology of PMMA/GO/PPy-A and B precursors was investigated by SEM analysis. As shown in Fig. 2a, PMMA/GO/PPy-A presents welldefined spherical particles with diameters ranging from 250 to 300 nm. However, the PMMA/GO/PPy-B precursor presents less-defined spherical particles than PMMA/GO/PPy-A (Fig. 2b). The increase in PPy content in PMMA/GO/PPy system increases the thickness of the PPy coating on the PMMA particles, inducing particles aggregation and less-defined morphology.

Published in : J Mater Sci (2018), vol. 53, pp. 6135-6146
DOI: 10.1007/s10853-017-1974-9
Status : Postprint (Author's version)

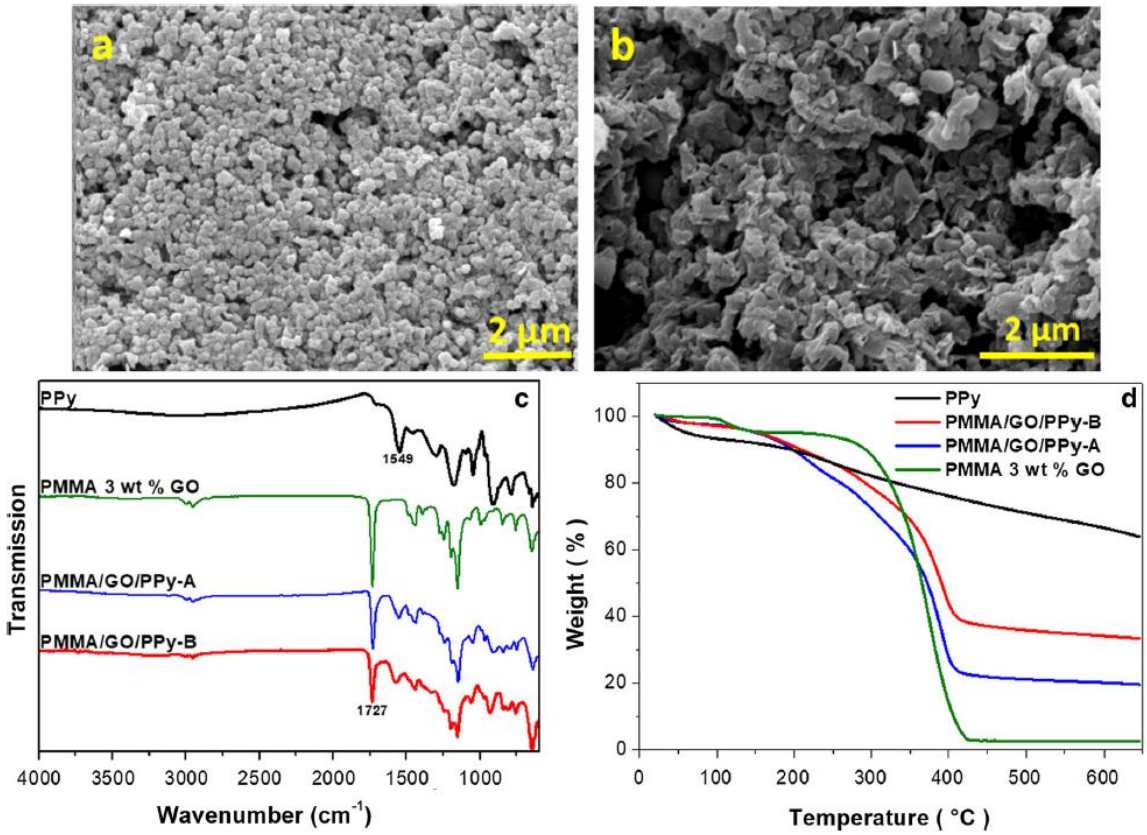

Figure 2 SEM image of a PMMA/GO/PPy-A and b PMMA/GO/PPy-B, c FTIR-ATR spectra and d TGA thermograms of PPy, PMMA/ GO (3 wt%), PMMA/GO/PPy-A and PMMA/GO/PPy-B under N_2 atmosphere.

The chemical structure and composition of both N-doped carbon precursors was investigated by FTIR-ATR and TGA analysis under nitrogen. The FTIR-ATR spectra of PPy, PMMA/3 wt%GO, PMMA/GO/PPy-A and PMMA/GO/PPy-B are superimposed in Fig. 2c. The characteristic peaks of PMMA/GO (C–O at 1147 cm^{-1}, C–O–C at 1435 cm^{-1} and C=O at 1727 cm^{-1}) and the characteristic peaks of PPy (alkane (C–H) deformation at 1455 cm^{-1}, alkane (C–H) bend vibration between 500 and 1000 cm^{-1}, N–H deformation at 1549 cm^{-1}) [24]–[26] are all observed in the spectra of PMMA/GO/PPy-A and PMMA/GO/PPy-B. TGA measurements were taken with the two NPC precursors (PMMA/GO/ PPy-A and PMMA/GO/PPy-B) in a N_2 atmosphere and compared with the PMMA/3 wt% GO sample and pristine PPy (Fig. 2d). Significant weight losses are observed for the PMMA/GO template (green line) between 200 and 400 °C, which is attributed to the decomposition of PMMA chains. A residue of around 3.3 wt% is measured which corresponds to the graphene present in the PMMA/GO template. A residue of more than 64 wt% is observed for the pristine PPy (black line) due to the pyrolysis of PPy. For both NPC precursors (blue and red line), 20 and 33 wt% of residual carbon are measured for PMMA/ GO/PPy-A and PMMA/GO/PPy-B, respectively. As expected, the increase in PPy content in PMMA/GO/ PPy-B increases the percentage of residual carbon after pyrolysis. These results demonstrate clearly the successful incorporation of PPy in both NPC precursors and confirm the increase in PPy content in the PMMA/GO/PPy-B compared to the PMMA/GO/PPy-A.

Published in : J Mater Sci (2018), vol. 53, pp. 6135-6146
DOI: 10.1007/s10853-017-1974-9
Status : Postprint (Author's version)

The third step (Scheme 1) toward nitrogen-doped porous carbon materials consists in the pyrolysis of PMMA/GO/PPy-A and PMMA/GO/PPy-B precursors to yield NPC-A-700 and NPC-B-700, respectively. Both precursors were pyrolyzed by two heating steps under a N_2 atmosphere. The first step at 400 C induces the thermal degradation of the sacrificial PMMA concomitant to the thermal reduction of GO into graphene nanosheets [27]. The second step at 700 °C induces the pyrolysis of the PPy matrix [28]. The morphology of the collected NPCs after pyrolysis at elevated temperatures was investigated by SEM (Fig. 3a, b). A continuous carbon network with a regular open macroporous structure is remarkably observed for both samples. The diameters of the pores are in the range of 200–250 nm, which is close to that of the PMMA particles. This tends to confirm that the pores are generated by the degradation of the PMMA sacrificial particles as described on Scheme 1. To confirm this assumption, we observed the morphology of PMMA/GO/PPy-A after the first heating step at 400 C (Fig. 3c, NPC-A-400). This image already shows a porous continuous matrix with defined macropores of 200–300 nm in diameter, i.e., the diameter of PMMA/GO particles, confirming the proposed mechanism of macroporosity design. This macroporous structure is then reinforced by the pyrolysis of the PPy at 700 °C (for NPC-A-700 and NPC-B-700). Furthermore, the increase in PPy content in PMMA/GO/PPy-B precursor gives NPC-B-700 that exhibits a porous carbon matrix with thicker walls but still well-defined macropores (Fig. 3b). To highlight the role of the PMMA particles on the formation process of porous carbon, experiments have been performed under the same conditions without PMMA (NC-rGO). Figure 3d shows SEM images of NC-rGO obtained after the thermal treatment of PPy/GO at 400 and 700 °C under a N_2 atmosphere. NC-rGO shows the presence of carbon materials without any visible porosity. The presence of PMMA particles stabilized by GO sheets plays a crucial role for the formation of continuous 3D carbon matrix with controlled macropores. The size of the macropores appears thus driven by the PMMA particles size. The N-doping level of NPC-A-700 and NPC-B-700 was checked by elemental analysis (Table 1). The results provided in Table 1 show 7.46 and 4.22 wt% of nitrogen content for NPC-A-700 and NPC-B-700, respectively. The increase in PPy amount versus PMMA/GO in the reaction mixture allows to increase the N-doping level of NPCs materials. The high nitrogen content in the porous carbon materials might be beneficial to develop more lithium-ion storage sites and further enhance the electronic conductivity, which can enhance the performance of the electrode materials [4].

Nitrogen adsorption isotherms obtained at 77 K for NPC-A-700, NPC-B-700, NPC-A-400 and NC-rGO are shown in Fig. 4a and their Brunauer–Emmett–Teller (BET) specific surface area (S_{BET}) and micropore volume, determined by the Dubinin–Radushkevich model (V_{DUB}), are listed in Table 1. Hysteresis loops in the relative pressure of P/P_0 = 0.5 - 0.98 are observed on the N_2 adsorption–desorption isotherm for NPC-A-700 and NPC-A-400, indicating the existence of mesopores and macropores [24], [29], [30]. NPCA-700 and NPC-A-400, which have the same PMMA/PPy ratio, present comparable specific surface area values, i.e., 398 and 397 m^2/g, respectively.

Published in : J Mater Sci (2018), vol. 53, pp. 6135-6146
DOI: 10.1007/s10853-017-1974-9
Status : Postprint (Author's version)

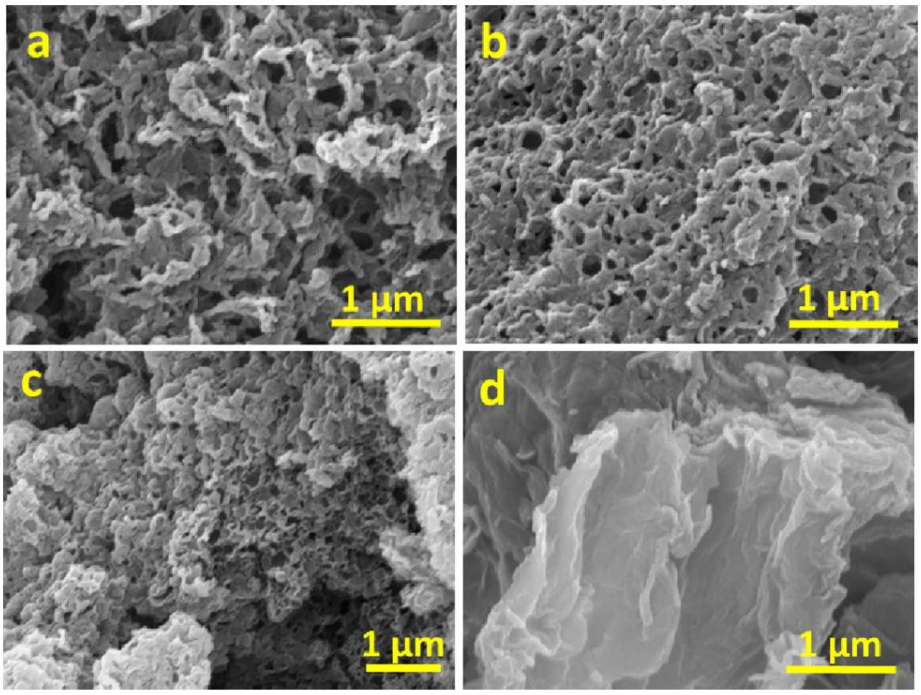

Figure 3 SEM images of a NPC-A-700, b NPC-B-700, c NPC-A-400 and d NC-rGO.

Table 1 Textural features and pyrolysis condition of the different carbon NPCs

Sample	Py/GO (wt/wt%)	Conditions of pyrolysis	*N* (wt%)	S_{BET} (m^2/g)[a]	V_{DUB} (cm^3/g)[a]
NPC-A-700	2/1	400 °C/1 h (5 °C/min) + 700 °C/1 h (5 °C/min)	4.22	398	0.16
NPC-B-700	4/1	400 °C/1 h (5 °C/min) + 700 °C/1 h (5 °C/min)	7.46	289	0.12
NPC-A-400	2/1	400 °C/1 h (5 °C/min)	–	397	0.16
NC-rGO[b]	2/1	400 °C/1 h (5 °C/min) + 700 °C/1 h (5 °C/min)	–	196	0.08

[a]BET surface area and micropore volume reported per mass unit of composite material (graphene + N-doped-carbon)

[b]NC-rGO was obtained in absence of PMMA particles

The rather large surface areas originate from a significant amount of meso- and macropores generated by the degradation of PMMA template and the pyrolysis (or cyclization at 400 °C for NPC-A-400) of PPy. Due to the increase in PPy content in the PMMA/GO/PPy-B precursor, NPC-B-700 exhibits less pronounced hysteresis loop and lower surface area (289 m^2/g). NC-rGO, obtained from the pyrolysis of PPy/GO composite (without PMMA particles template), displays a very low specific surface area (196 m^2/g) compared to NPC-A-700 (397 m^2/g) and NPC-B-700 (289 m^2/g), obtained in presence of PMMA particles. The corresponding pore size distribution of NPCs (Figure S3) confirms the existence of small mesopores in the range of 3–5 nm in all samples.

Published in : J Mater Sci (2018), vol. 53, pp. 6135-6146
DOI: 10.1007/s10853-017-1974-9
Status : Postprint (Author's version)

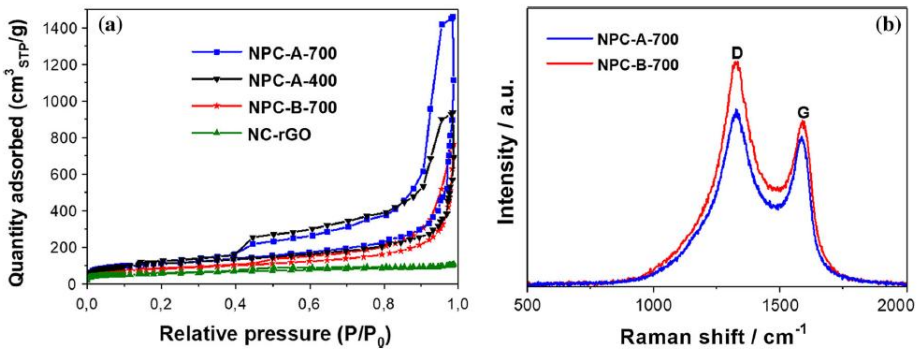

Figure 4 a Nitrogen adsorption–desorption isotherms of NPC-A-700, NPC-A-400, NPC-B-700 and NC-rGO, reported per mass unit of composite and b Raman spectra of NPC-A-700 and NPC-B-700.

However, larger mesopores and macropores are completely absent in the non-templated sample (NC-rGO). This confirms the beneficial effect of PMMA/GO template in the porosity development process, which increases the surface area of the obtained carbon materials.

The carbon structures of the obtained NPC-A-700 and NPC-B-700 samples were characterized by Raman spectroscopy. One observes two broad characteristic peaks (1332 and 1594 cm^{-1}) in the Raman spectra (Fig. 4b) of NPC-A-700 and NPC-A-400, which correspond, respectively, to the disordered band (D), caused by the imperfect structures of carbon material, and the graphitic band (G), caused by the formation of sp^2 carbon [31]–[33]. The I_D/I_G values for NPC-A-700 and NPC-B-700 were 1.18 and 1.35, respectively, which demonstrates a higher disorder degree compared to crystalline graphite-based materials [34], [35]. The enhanced disorder degree of NPCs samples may be related to the inherent nitrogen atoms, which prevent the formation of sp^2 carbons and promote the growing of an imperfect structure during the pyrolysis process. Furthermore, the absence of PPy-related bands around 1000 cm^{-1} suggests that the PPy has been successfully pyrolyzed [36]. The high disorder degree of NPC structure was then confirmed by XRD measurements (Figure S4). NPC-A-700 and NPC-B-700 exhibit similar XRD diffraction features with just a broad peak at approximately 2θ = 19°, which demonstrates that NPC-A-700 and NPC-B-700 samples are amorphous. The obtained NPC is composed of disorganized graphene sheet in the core covered by amorphous N-doped carbon layer.

The electrochemical performances of NPC were investigated in a half-cell configuration with the lithium plate as the counter-electrode. To evaluate the electrochemical performances of NPC, their galvanostatic discharge/charge behaviors in the potential range from 0.005 to 1.5 V at a rate of C/5 (1C = 372 mA/g) were measured by considering all the composite material (graphene + N-doped-carbon) as active material. In other words, all capacities (mAh/g) are reported per mass unit of composite. The charge/discharge capacity and cycling performances of NPC-A-700, NPC-A-400 and NC-rGO at 74.4 mA/g (C/5) of current density are shown in Fig. 5a. NPC-A-700 and NPC-A-400 present higher initial capacity (2910 and 2530 mAh/g) compared to NC-rGO (830 mAh/g). These high initial capacities are related to the irreversible reaction of the electrolyte to form a solid electrolyte interface (SEI) layer [4], [35]. The highly accessible graphene nanosheets in NPCs especially after

Published in : J Mater Sci (2018), vol. 53, pp. 6135-6146
DOI: 10.1007/s10853-017-1974-9
Status : Postprint (Author's version)

thermal treatment in the presence of N atoms creating a large number of defects increases the ratio between the edge carbon and a surface of the basal plane, which might explain the high initial discharge capacity [37]. After 50 cycles of discharge/charge, the reversible capacity of NPC-A700 (399 mAh/g) is almost twice higher than the one of NPC-A-400 (205 mAh/g) and NC-rGO (195 mAh/ g). These higher performances of NPC-A-700 compared to NPC-A-400 and NC-rGO highlight two important parameters: the effect of PPy pyrolysis temperature (700 °C) and the importance of the hierarchical meso/macroporous structure. Indeed, the continuous carbon network of NPC-A-700 with meso- and macropores and high surface area can offer large electrolyte/electrode interface for charge transfer reaction and more Li^+ insertion sites [32].

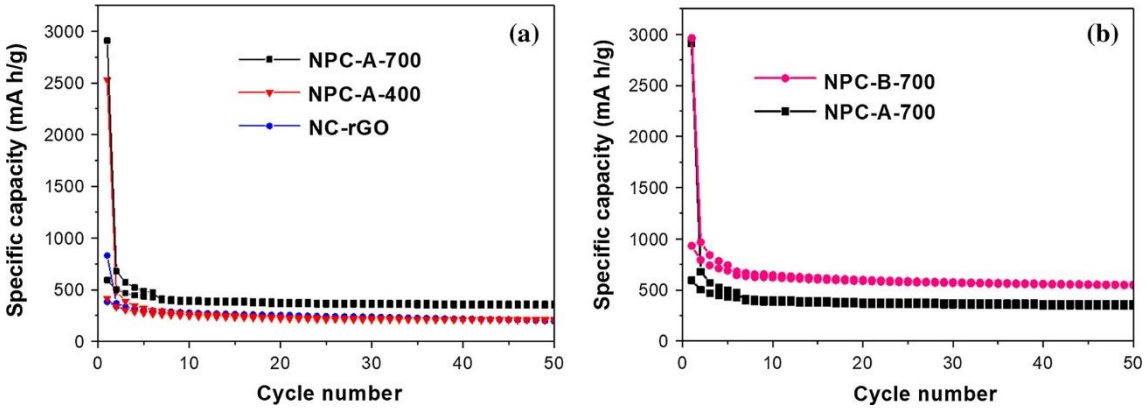

Figure 5 Cycling performances at a current density of 74.4 mA/g (1C = 372 mA/g) in the potential range from 0.005 to 1.5 V of a NPC-A-700 (black), NPC-A-400 (red) and NC-rGO (blue), b NPC-A-700 (black) and NPC-B-700 (pink). Performances are reported per mass unit of composite (graphene + N-dopedcarbon), considered as the active material.

To better evidence the importance of the nitrogen content for the electrochemical properties, we compared the charge/discharge cycling capacities of NPC-A700 (containing 4.22 wt% of N) and NPC-B-700 (7.46 wt% of N) at a current density of C/5 between 0.005 and 1.5 V (Fig. 5b). After 50 cycles of charge/ discharge, NPC-B-700 shows high reversible capacity of 541 mAh/g, which is 35% higher than the capacity obtained with NPC-A-700 (399 mAh/g). This increase in specific capacity can be related to the increased N-doping level (7.46 wt% of N) in NPC-B700, which is beneficial for the enhancement of Li^+ sites storage [4]. Indeed, the incorporation of N atoms in graphitic carbon generates pyrrolic and pyridinic groups that are able to provide a larger number of active sites for Li-ion adsorption by increasing the number of defects in the carbon lattice [4]. The rate performances of NPC-B-700 at different current densities (C/5, C/2, 1C and 2C) between 0.005 and 1.5 V versus Li^+/Li, compared with those of NPC-A700 (as presented in Figure S5) confirm the beneficial effect of the increasing of N-doping level.

To compare with reported N-doped carbons in the literature, the electrochemical performances of the best candidate, NPC-B-700, were investigated by galvanostatic discharge/charge in the voltage range of 0.005–3.0 V (vs. Li^+/Li) at the current density of 74.4 mA/g. To get as close as possible to conditions found in previous studies [22], [39], the mass loading of the electrode was increased to 0.9 mg/cm^2 (instead of 0.5 mg/cm^2 used previously in the voltage range of 0.005–1.5 V). However, it must be pointed out that the increase in the mass loading may decrease the accessibility of the

Published in : J Mater Sci (2018), vol. 53, pp. 6135-6146
DOI: 10.1007/s10853-017-1974-9
Status : Postprint (Author's version)

active materials, which in turn can affect the measured capacities. Indeed, a lack of contact between the electrode and the electrolyte, typical of high mass loadings, leads to an underestimation of the (irreversible and reversible) capacities[38].

The discharge–charge voltage-capacity profiles of NPC-B-700 electrode for the first, second, third and 50th cycles are presented in Fig. 6a. The discharge/ charge curves of NPC-B-700 exhibit no voltage plateau, due to the presence of a large amount of disordered carbon atoms [39]. As expected, the first discharge–charge curves of NPC-B-700 show high initial discharge capacity (2039 mAh/g) compared to second cycle (866 mAh/g) due to the formation of the SEI film at the electrode–electrolyte interface. However, the reversible capacity of NPC-B-700 remains stable at 831 mAh/g after the 50th cycle at C/5 of current speed (Fig. 6b). The coulombic efficiency increases from 42.5% in the first cycle to 88.3% for the 2nd cycle and exceeds 97.1% after 10 cycles. This excellent electrochemical performance of NPC-B-700 could be due to their unique interconnected hierarchical meso/macroporous structure and high N-doped level. Note, however, that the insertion capacity at the first cycle is lower than previously (i.e., when the same material was cycled between 0.005 and 1.5 V vs. Li^+/Li): ~ 2000 mAh/g versus 3000 mAh/g. Similarly, the charge capacity (i.e., upon deinsertion) observed at 1.5 V in Fig. 6a is much lower (~ 650 mAh/g) than previously (~ 1000 mAh/g, see capacity at the second cycle in Fig. 5b).

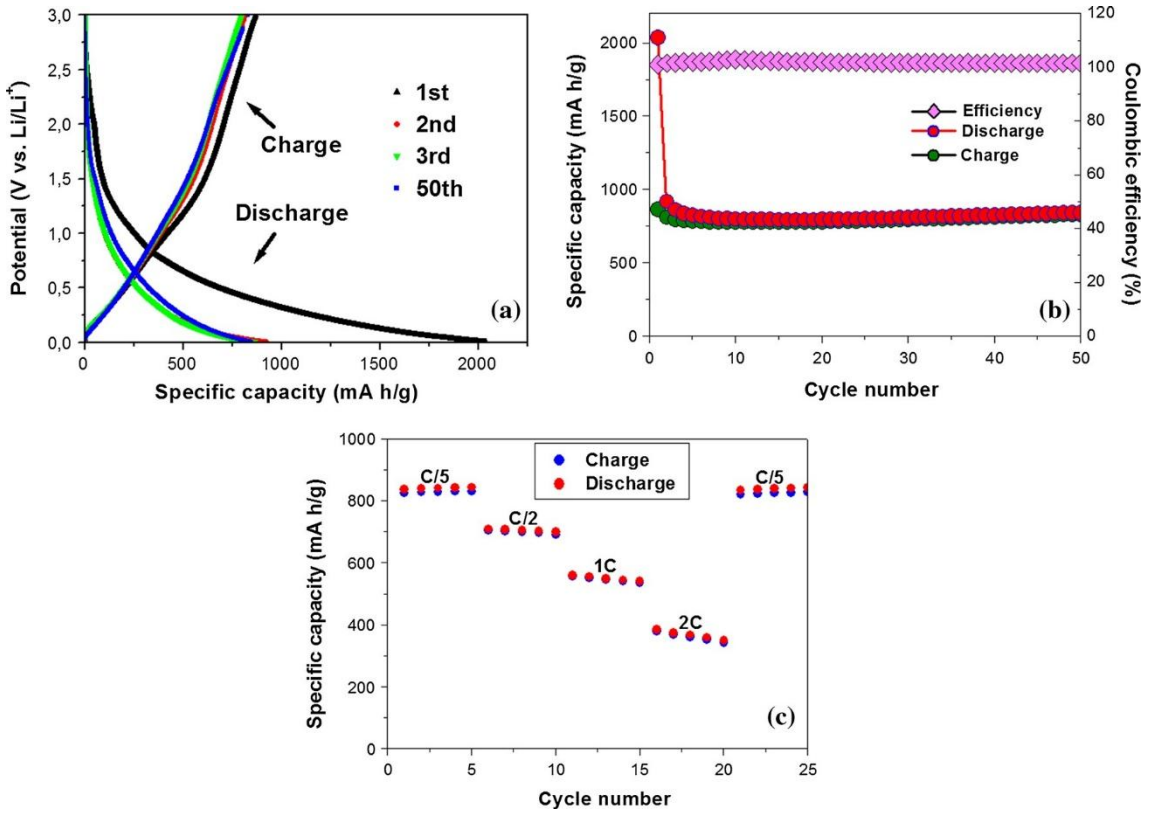

Figure 6 a Discharge and charge voltage profiles of the NPC-B700, b cycling performance of NPC-B-700 at a current density of 74.4 mA/g and c rate performance at different current densities of C/5, C/2, 1C and 2C. All measurements are carried out in the voltage range of 0.005–3.0 V versus Li/Li^+. Performances are reported per mass unit of composite (graphene + N-dopedcarbon), considered as the active material.

Published in : J Mater Sci (2018), vol. 53, pp. 6135-6146
DOI: 10.1007/s10853-017-1974-9
Status : Postprint (Author's version)

This hints a possible lack of contact between the active material and the electrolyte when the loading is increased up to 0.9 mg/cm^2. These results indicate that (1) measuring properly the specific capacity of a material is not straightforward and that (2) comparison is not easy between various studies, owing to the various conditions used (among which the potential window and electrode loading).

The rate capability and the long cycling stability are the important parameters for LIBs. Figure 6c shows the rate performance of NPC-B-700 at different current densities, i.e., C/5, C/2, 1C and 2C (1C = 372 mA/g), followed by galvanostatic cycling at C/5. It is found that NPC-B-700 exhibits a robust rate performance with a reversible capacity of 831, 691, 535 and 343 mAh/g at C/5, C/2, 1C and 2C, respectively. The good rate performance of NPC-B700 anode confirms the beneficial effect of the combination of the high N-doping level and continuous carbon network with hierarchical meso/macroporous structure, which induces a large surface area that offers a large electrode/electrolyte interface, shortens the Li^+ transport length and increases Li^+ sites storage. These electrochemical performances of NPC-B-700 are comparable to or even better than other porous N-doped carbon systems reported in recent publications [22], [34], [40]–[42]. The uniqueness in our approach lies in the particular employment of two compartmentalized polymers, i.e, the colloidal PMMA particles as core and polypyrrole as shell, the former serving to produce large pore highways for fast mass transport while the latter induces the formation of mesoporous N-doped carbon to increase the Li^+ sites storage.

Conclusion

N-doped continuous network carbon materials (NPCs) with hierarchical meso/macroporous structure have been prepared by pyrolysis of PMMA/ GO / PPy precursor using polypyrrole as N-doped carbon source and PMMA/graphene oxide particles as templates. The reported synthetic strategy was conducted in aqueous medium, which should ease the process scale up. The resulting materials exhibit high specific surface area up to 398–289 m^2/g and high N-doping level up to 7.46 wt%. Electrochemical measurements showed that the NPCs possess promising performance in a Li-ion battery. The best sample among the series was identified as NPC-B-700 with high N-doping level (7.46 wt%), which preserves high capacity of 831 mAh/g at the current rate of C/5 even after 50 cycles.

Acknowledgements

CERM is much indebted to BELSPO Interuniversity Attraction Poles (IAP-7/5-FS2) for financial support in the frame of ''Functional Supramolecular Systems'' project. C. D. is Research Director by the FRS-FNRS.

Electronic supplementary material: The online version of this article (https://doi.org/10.1007/s10853-017-1974-9) contains supplementary material, which is available to authorized users.

Published in : J Mater Sci (2018), vol. 53, pp. 6135-6146
DOI: 10.1007/s10853-017-1974-9
Status : Postprint (Author's version)

References

[1] Armand M, Tarascon J-M (2008) Building better batteries. Nature 451:652–657

[2] Tarascon J-M, Armand M (2001) Issues and challenges facing rechargeable lithium batteries. Nature 414:359–367

[3] Kang B, Ceder G (2009) Battery materials for ultrafast charging and discharging. Nature 458:190–193

[4] Wu Z-S, Ren W, Xu L et al (2011) Doped graphene sheets as anode materials with superhigh rate and large capacity for lithium ion batteries. ACS Nano 5:5463–5471

[5] Chen T, Pan L, Liu X, Sun Z (2013) A comparative study on electrochemical performances of the electrodes with different nanocarbon conductive additives for lithium ion batteries. Mater Chem Phys 142:345–349

[6] Guo X, Wang C, Chen M et al (2012) Carbon coating of Li4Ti5O12 using amphiphilic carbonaceous material for improvement of lithium-ion battery performance. J Power Sources 214:107–112

[7] Deng D (2015) Li-ion batteries: basics, progress, and challenges. Energy Sci Eng 3:385–418

[8] Inagaki M, Yang Y, Kang F (2012) Carbon nanofibers prepared via electrospinning. Adv Mater 24:2547–2566

[9] Li M, Carter R, Cohn AP, Pint CL (2016) Interconnected foams of helical carbon nanofibers grown with ultrahigh yield for high capacity sodium ion battery anodes. Carbon 107:109–115

[10] Liu X-M, dong Huang Z, woon Oh S et al (2012) Carbon nanotube (CNT)-based composites as electrode material for rechargeable Li-ion batteries: a review. Compos Sci Technol 72:121–144

[11] Qu Y, Zhang Z, Du K et al (2016) Synthesis of nitrogencontaining hollow carbon microspheres by a modified template method as anodes for advanced sodium-ion batteries. Carbon 105:103–112

[12] Fang Y, Lv Y, Che R et al (2013) Two-dimensional mesoporous carbon nanosheets and their derived graphene nanosheets: synthesis and efficient lithium ion storage. J Am Chem Soc 135:1524–1530

[13] Tang J, Chen G, Yang J et al (2014) Silica-assistant synthesis of three-dimensional graphene architecture and its application as anode material for lithium ion batteries. Nano Energy 8:62–70

[14] Strubel P, Althues H, Kaskel S (2016) Zinc-salt templating of hierarchical porous carbons for low electrolyte high energy lithium-sulfur batteries (LE-LiS). Carbon 107:705–710

[15] Qie L, Chen W, Wang Z et al (2012) Nitrogen-doped porous carbon nanofiber webs as anodes for lithium ion batteries with a superhigh capacity and rate capability. Adv Mater 24:2047–2050

[16] Kim MG, Cho J (2009) Reversible and high-capacity nanostructured electrode materials for li-ion batteries. Adv Func Mater 19:1497–1514

[17] Sun D, Yang J, Yan X (2015) Hierarchically porous and nitrogen, sulfur-codoped graphene-like microspheres as a high capacity anode for lithium ion batteries. Chem Commun 51:2134–2137

[18] Deng D, Pan X, Yu L et al (2011) Toward N-doped graphene via solvothermal synthesis. Chem Mater 23:1188–1193

[19] Panchakarla LS, Subrahmanyam KS, Saha SK et al (2009) Synthesis, structure, and properties of boron- and nitrogendoped graphene. Adv Mater 21:4726–4730

[20] Zhou X, Tang J, Yang J et al (2013) Seaweed-like porous carbon from the decomposition of polypyrrole nanowires for application in lithium ion batteries. J Mater Chem A 1:5037–5044

[21] Ma C, Shao X, Cao D (2012) Nitrogen-doped graphene nanosheets as anode materials for lithium ion batteries: a first-principles study. J Mater Chem 22:8911–8915

[22] Liu X, Zhang J, Guo S, Pinna N (2016) Graphene/N-doped carbon sandwiched nanosheets with ultrahigh nitrogen doping for boosting lithium-ion batteries. J Mater Chem A 4:1423–1431

[23] Thomassin J-M, Trifkovic M, Alkarmo W et al (2014) Poly(methyl methacrylate)/graphene oxide nanocomposites by a precipitation polymerization process and their dielectric and rheological characterization. Macromolecules 47:2149–2155

Published in : J Mater Sci (2018), vol. 53, pp. 6135-6146
DOI: 10.1007/s10853-017-1974-9
Status : Postprint (Author's version)

[24] Zhang D, Dong Q-Q, Wang X et al (2013) Preparation of a three-dimensional ordered macroporous carbon nanotube/ polypyrrole composite for supercapacitors and diffusion modeling. J Phys Chem C 117:20446–20455

[25] Muylaert I, Verberckmoes A, De Decker J, Van Der Voort P (2012) Ordered mesoporous phenolic resins: highly versatile and ultra stable support materials. Adv Coll Interface Sci 175:39–51

[26] Bulusheva LG, Okotrub AV, Kurenya AG et al (2011) Electrochemical properties of nitrogen-doped carbon nanotube anode in Li-ion batteries. Carbon 49:4013–4023

[27] Pei S, Cheng H-M (2012) The reduction of graphene oxide. Carbon 50:3210–3228

[28] Li D, Ding L-X, Chen H et al (2014) Novel nitrogen-rich porous carbon spheres as a high-performance anode material for lithium-ion batteries. J Mater Chem A 2:16617–16622

[29] Tripathi PK, Liu M, Zhao Y et al (2014) Enlargement of uniform micropores in hierarchically ordered micro-mesoporous carbon for high level decontamination of bisphenol A. J Mater Chem A 2:8534–8544

[30] Tripathi PK, Gan L, Liu M et al (2014) One-pot assembly of silica@two polymeric shells for synthesis of hollow carbon porous nanospheres: adsorption of bisphenol A. Mater Lett 120:108–110

[31] Ferrari AC, Meyer JC, Scardaci V et al (2006) Raman spectrum of graphene and graphene layers. Phys Rev Lett 97:187401

[32] Song R, Song H, Zhou J et al (2012) Hierarchical porous carbon nanosheets and their favorable high-rate performance in lithium ion batteries. J Mater Chem 22:12369–12374

[33] Ferrari AC, Robertson J (2000) Interpretation of Raman spectra of disordered and amorphous carbon. Phys Rev B 61:14095–14107

[34] Li X, Zhu X, Zhu Y et al (2014) Porous nitrogen-doped carbon vegetable-sponges with enhanced lithium storage performance. Carbon 69:515–524

[35] Wang G, Shen X, Yao J, Park J (2009) Graphene nanosheets for enhanced lithium storage in lithium ion batteries. Carbon 47:2049–2053

[36] Liu Y, Liu X, Chen J et al (2008) 3D bio-nanofibrous PPy/ SIBS mats as platforms for cell culturing. Chem Commun. https://doi.org/10.1039/b804283g

[37] Omichi K, Ramos-Sanchez G, Rao R et al (2015) Origin of excess irreversible capacity in lithium-ion batteries based on carbon nanostructures. J Electrochem Soc 162:A2106– A2115

[38] Piedboeuf M-LC, Le´onard AF, Deschamps FL, Job N (2016) Carbon xerogels as model materials: toward a relationship between pore texture and electrochemical behavior as anodes for lithium-ion batteries. J Mater Sci 51:4358–4370. https:// doi.org/10.1007/s10853-016-9748-3

[39] Jiang Z-J, Jiang Z (2014) Fabrication of nitrogen-doped holey graphene hollow microspheres and their use as an active electrode material for lithium ion batteries. ACS Appl Mater Interfaces 6:19082–19091

[40] Liu C, Liu X, Tan J et al (2017) Nitrogen-doped graphene by all-solid-state ball-milling graphite with urea as a high-power lithium ion battery anode. J Power Sources 342:157–164

[41] Nan D, Huang Z-H, Lv R et al (2014) Nitrogen-enriched electrospun porous carbon nanofiber networks as high-performance free-standing electrode materials. J Mater Chem A 2:19678–19684

[42] Tan G, Bao W, Yuan Y et al (2017) Freestanding highly defect nitrogen-enriched carbon nanofibers for lithium ion battery thin-film anodes. J Mater Chem A 5:5532–5540